## Title
Early role for a Na+,K+-ATPase (ATP1A3) in brain development



## Journal
Proceedings of the National Academy of Sciences of the United States of America, 118(25)

## ISSN
0027-8424

## Authors
Smith, Richard S
Florio, Marta
Akula, Shyam K
et al.

## Publication Date
2021-06-22

## DOI
10.1073/pnas.2023333118

Peer reviewed

# Early role for a $Na^+,K^+$-ATPase (*ATP1A3*) in brain development

Richard S. Smith[a,b,1], Marta Florio[c,d], Shyam K. Akula[a,b,e], Jennifer E. Neil[a,b], Yidi Wang[a,b], R. Sean Hill[a,b], Melissa Goldman[c,d], Christopher D. Mullally[c,d], Nora Reed[c,d], Luis Bello-Espinosa[f], Laura Flores-Sarnat[g], Fabiola Paoli Monteiro[h], Casella B. Erasmo[i], Filippo Pinto e Vairo[j,k], Eva Morava[i], A. James Barkovich[l,m,n], Joseph Gonzalez-Heydrich[o], Catherine A. Brownstein[a,b], Steven A. McCarroll[c,d], and Christopher A. Walsh[a,b,1]

[a]Division of Genetics and Genomics, Manton Center for Orphan Disease Research, Howard Hughes Medical Insitute, Boston Children's Hospital, Boston, MA 02115; [b]Department of Pediatrics and Neurology, Broad Institute of MIT and Harvard, Harvard Medical School, Boston, MA 02115; [c]Department of Genetics, Harvard Medical School, Boston, MA 02115; [d]Stanley Center for Psychiatric Research, Broad Institute of MIT and Harvard, Cambridge, MA 02142; [e]Harvard-MIT MD/PhD Program, Program in Neuroscience, Harvard Medical School, Boston, MA 02115; [f]Arnold Palmer Hospital for Children, Orlando, FL 32806; [g]Department of Paediatrics and Clinical Neurosciences, The Owerko Centre, University of Calgary and Alberta Children's Hospital Research Institute, Calgary, AB T2N 1N4, Canada; [h]Mendelics Genomic Analysis, CEP 04013-000 São Paulo, Brazil; [i]Children's Institute, Hospital das Clinicas, CEP 05403-000 São Paulo, Brazil; [j]Center for Individualized Medicine, Mayo Clinic, Rochester, MN 55905; [k]Department of Clinical Genomics, Mayo Clinic, Rochester, MN 55905; [l]Department of Radiology, Benioff Children's Hospital, University of California, San Francisco, CA 94117; [m]Department of Pediatrics, Benioff Children's Hospital, University of California, San Francisco, CA 94117; [n]Department of Neurology, Benioff Children's Hospital, University of California, San Francisco, CA 94117; and [o]Department of Psychiatry, Boston Children's Hospital, Harvard Medical School, Boston, MA 02115

Contributed by Christopher A. Walsh, April 5, 2021 (sent for review December 1, 2020; reviewed by Simon Hippenmeyer and Denis Jabaudon)

**Osmotic equilibrium and membrane potential in animal cells depend on concentration gradients of sodium ($Na^+$) and potassium ($K^+$) ions across the plasma membrane, a function catalyzed by the $Na^+,K^+$-ATPase α-subunit. Here, we describe *ATP1A3* variants encoding dysfunctional α3-subunits in children affected by polymicrogyria, a developmental malformation of the cerebral cortex characterized by abnormal folding and laminar organization. To gain cell-biological insights into the spatiotemporal dynamics of prenatal *ATP1A3* expression, we built an *ATP1A3* transcriptional atlas of fetal cortical development using mRNA in situ hybridization and transcriptomic profiling of ∼125,000 individual cells with single-cell RNA sequencing (Drop-seq) from 11 areas of the midgestational human neocortex. We found that fetal expression of *ATP1A3* is most abundant to a subset of excitatory neurons carrying transcriptional signatures of the developing subplate, yet also maintains expression in nonneuronal cell populations. Moving forward a year in human development, we profiled ∼52,000 nuclei from four areas of an infant neocortex and show that *ATP1A3* expression persists throughout early postnatal development, most predominantly in inhibitory neurons, including parvalbumin interneurons in the frontal cortex. Finally, we discovered the heteromeric $Na^+,K^+$-ATPase pump complex may form nonredundant cell-type–specific α-β isoform combinations, including α3-β1 in excitatory neurons and α3-β2 in inhibitory neurons. Together, the developmental malformation phenotype of affected individuals and single-cell *ATP1A3* expression patterns point to a key role for α3 in human cortex development, as well as a cell-type basis for pre- and postnatal *ATP1A3*-associated diseases.**

cortex development | ATP1A3 | developmental channelopathy | polymicrogyria | cortical malformation

Generating a folded, six-layered cerebral cortex relies on the integration of signals from a variety of cell types, coordinating schedules of cell proliferation, migration, differentiation, and maturation. These processes require proper maintenance of ionic gradients and cell membrane potential (Vm) and thus rely on the precise function of ion channels and pumps. Pathogenic mutations in genes encoding ion channels can cause malformations of cortical development (MCDs), collectively known as prenatal developmental channelopathies (1). For example, pathogenic variants in prenatally expressed genes encoding glutamate (*GRIN2B*, *GRIN1*) and sodium channels (*SCN3A*) can lead to MCDs (2–4), at least in part via gain-of-function, cell-autonomous effects in neurons and other cell types (4). These developmental channelopathy variants in glutamate and sodium channels cause pathogenic increases in cationic flux into cells (1), likely affecting Vm in neural progenitor cells (NPCs) and neurons, a perturbation shown to be sufficient to disrupt neurogenic and cortical lamination processes in experimental models (5, 6).

Neuronal physiology, homeostasis, and signaling depend on the electrogenic activity of the $Na^+,K^+$-ATPase, an ionic pump powered by ATP hydrolysis, which maintains sodium ($Na^+$) and potassium ($K^+$) gradients across the plasma membrane. The Na,K-ATPase complex contains a large catalytic subunit (α) and two auxiliary subunits (β, FXYD) (7). In vertebrates, paralogous genes (*ATP1A1* to *-3*) encode the brain enriched α-subunits and the *ATP1A3* isoform specifically is critical for recovery of electrochemical gradients following neuronal excitation, among several other physiological functions (8–10). Pathogenic variants in *ATP1A3* have been increasingly associated with a spectrum of neurological diseases, with phenotypes ranging broadly in age of onset from the immediate postnatal period throughout adulthood

## Significance

By evaluating children with a malformed cerebral cortex, we identified an ATPase pump (ATP1A3) with an early role in brain development. The ATP1A3 pump maintains the physiological concentration of sodium and potassium ions in cells, a process critical for osmotic equilibrium and membrane potential across several developing cell populations. We employed single-cell sequencing approaches to identify key enrichments for *ATP1A3* expression during human cortex development. Unravelling this early cell-type–specific pathophysiology in the developing brain offers a potential basis for the treatment of *ATP1A3*-related diseases affecting prenatal and early childhood development.

Author contributions: R.S.S, M.F., and C.A.W. designed research; R.S.S. and M.F. performed research; R.S.S., S.K.A., Y.W., R.S.H., A.J.B., J.G.-H., C.A.B., and C.A.W. analyzed data; L.B.-E., L.F.-S., F.P.M., C.B.E., F.P.e.V., and E.M. contributed clinical data; J.E.N. coordinated clinical data; M.F., M.G., C.D.M., N.R., and S.A.M. generated Drop-seq libraries and resources; and R.S.S., M.F., S.K.A., J.E.N., and C.A.W. wrote the paper.

Reviewers: S.H., Institute of Science and Technology Austria; and D.J., Massachusetts General Hospital-Harvard Medical School Center for Nervous System Repair.

The authors declare no competing interest.



[1]To whom correspondence may be addressed. Email: richard.smith@childrens.harvard.edu or christopher.walsh@childrens.harvard.edu.

This article contains supporting information online at https://www.pnas.org/lookup/suppl/doi:10.1073/pnas.2023333118/-/DCSupplemental.

Published June 14, 2021.

(11, 12), suggesting shifting vulnerabilities to different *ATP1A3* dysfunction during the several stages of childhood brain maturation. These diseases include (in approximate order of onset in childhood development): early infantile epileptic encephalopathy (EIEE); alternating hemiplegia of childhood (AHC); cerebellar ataxia, areflexia, pes cavus, optic atrophy, and sensorineural hearing loss (CAPOS); childhood onset schizophrenia; and rapid-onset dystonia-parkinsonism (RDP) (11, 12). Variants in *ATP1A3* associated with these postnatal diseases are generally categorized as heterozygous loss-of-function (LOF) single-nucleotide variants (7, 13) that, among other deficits, have been shown to lead to depolarized Vm, such as in neurons from AHC patients (14). This finding, along with findings that bioelectric changes during circuit development can dramatically alter both intrinsic trajectories of individual cells (15) and cortical lamination more broadly (5, 6), suggests that bioelectric alterations due to *ATP1A3* dysfunction during embryonic development could in part contribute to an early pathophysiology for both pre- and postnatal-associated *ATP1A3*-related neurological disorders.

Here, we present four individuals with novel de novo *ATP1A3* variants, resulting in polymicrogyria (PMG, the most common brain malformation) (16), epilepsy, and global developmental

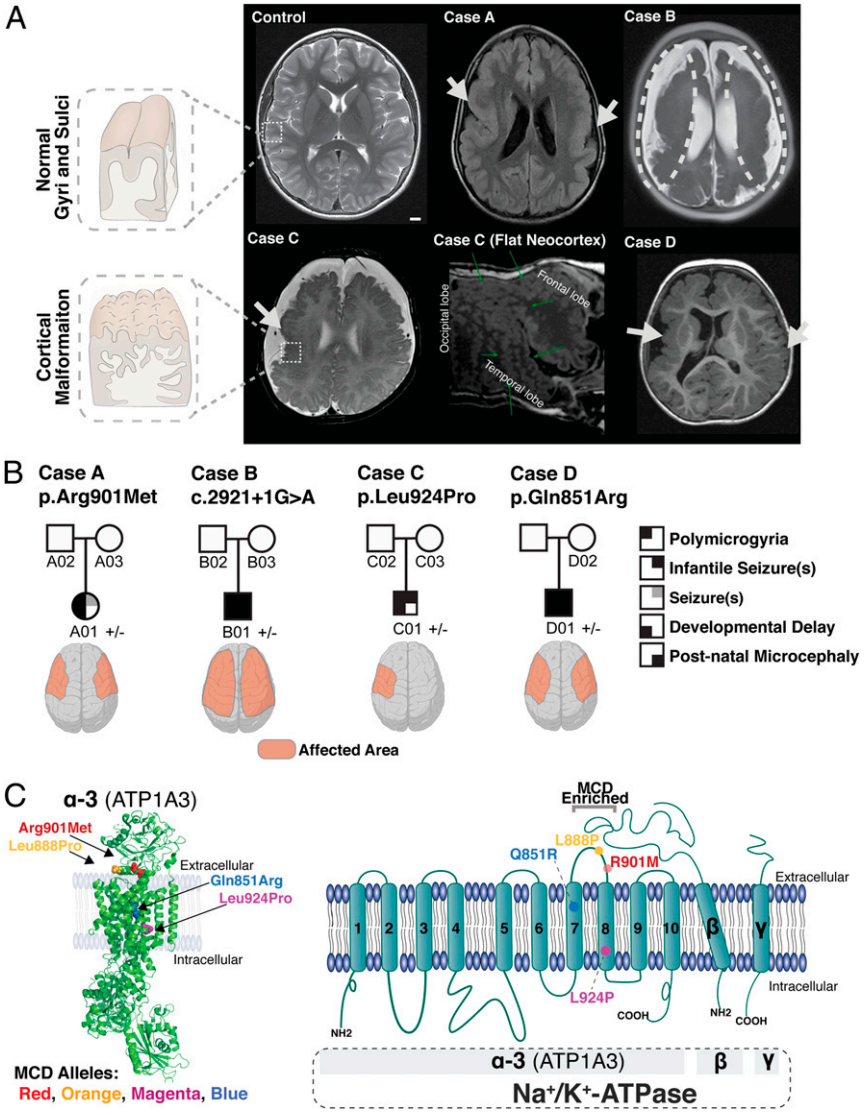


**Fig. 1.** *ATP1A3* variants associated with cerebral cortex malformations. (*A*, *Left*) Schematic of the cortical malformation, PMG, and resulting macroscopic disorganization of cortical gyri and sulci. (*Right*) MRI images of Cases A, B, C, and D showing PMG. White arrows denote gross location of affected brain regions. "Flat Neocortex" image provides alternative view of PMG surrounding the perisylvian region (green arrows) if the neocortex were unwrapped from around the subcortical structures and laid flat. The control image comes from an unaffected 11-y-old. (Scale bar, 1 cm.) (*B*) Pedigrees with novel de novo pathogenic single-nucleotide variants in *ATP1A3*: Case A (missense, p.Arg901Met) with bilateral frontoparietal PMG, Case B (splice donor site, c.2921+1G > A) with extensive bilateral PMG, Case C (missense, p.Leu924Pro) with unilateral PMG, and Case D (missense, p.Gly851Arg) with extensive bilateral PMG, more pronounced in the right hemisphere. Individual features: Genotype (±, de novo heterozygous), PMG, infantile seizures, developmental delay, and postnatal microcephaly shown in pedigree summary. Square, male; circle, female; black and/or gray shading, affected individual. See *SI Appendix* for genetic validation and comprehensive clinical phenotyping. (*C*) Overview of the α-subunit (green) of the Na,K-ATPase with novel PMG alleles mapped (colored amino acids) and previous case report of PMG-associated allele (Leu888Pro) (17). Red, p.Leu888Pro (L888P); orange, p.Arg901Met (R901M); magenta, p.Leu924Pro (L924P); blue, p.Gln851Arg (Q851R). Image generated with PyMOL using Protein Databank 2ZXE (21). (*Right*) TM topology schematic of Na,K-ATPase for visualization of PMG causing variants, including α-, β-, and FXYD-subunits. We also denote a variant enriched region TM7/TM8, where β-subunits interact with the α3-subunit in the extracellular TM7/TM8 segment Glu899, Gln904, and Gln905 (21). See *SI Appendix*, Figs. S7 and S8 and Table S4 for complete allele-to-protein topology breakdown.

delay, and consider a previously described individual report of AHC with PMG (17). Unlike *ATP1A3* variants associated with other conditions, the *ATP1A3* variants associated with PMG clustered in a "hotspot" between transmembrane regions 7 and 8 (TM7 and TM8) of the α3 protein. Using mRNA in situ analysis and single-cell RNA sequencing (scRNA-seq, Drop-seq) in the human fetal cortex at midgestation, we show that *ATP1A3* is most highly expressed in subset of deep-layer neurons located in the subplate (SP), and is also expressed in intermediate progenitors and neurons. We then show that the fetal cortex also displays a rostral-to-caudal *ATP1A3* gradient within SP excitatory neurons (ENs), with *ATP1A3* expression levels highest in the prefrontal cortex. Moreover, using Drop-seq in the human infant cortex, we show that postnatal expression of *ATP1A3* at this stage of development extends to all EN subtypes (with deeper layer cortical layer biases) and mostly predominates within cortical interneurons, most abundantly enriched to parvalbumin (PV) interneurons in the prefrontal cortex. Finally, within individual cells, variable levels of ATPase α- and β-subunit isoforms offers differential vulnerability between ENs and inhibitory neurons (INs), and may provide a partial explanation for the broad phenotypic range associated with distinct *ATP1A3* variants that affect different biological maturation processes within the pre- to postnatal period.

## Results

**Individuals with *ATP1A3* Variants Display Cortical Malformation Phenotypes.** MRI of four unrelated individuals with de novo *ATP1A3* variants revealed a range of PMG severity, from extensive bilateral frontoparietal PMG to unilateral PMG (Fig. 1*A*). Detailed descriptions of each case are included in *SI Appendix*, *Clinical Descriptions*.

***Case A: Bilateral frontoparietal PMG (p.Arg901Met).*** Case A, a female child of nonconsanguineous parents from Portugal, was born at full term and had a short postnatal hospital stay for respiratory distress and jaundice. Brain MRIs performed at 5 mo and at 9 y of age revealed extensive bilateral perisylvian PMG involving the lateral temporal lobes, insulae, and posterior half of frontal and parietal lobes (Fig. 1*A*). The posterior part of the frontal and temporal cortex appears abnormally thick, with somewhat shallow sulci, giving a pachygyric appearance (bilateral and fairly symmetrical, but with a mild left-to-right predominance). The most anterior aspects of the frontal and parietal lobes, as well as the medial and inferior cerebral cortex, were spared. At 9 y she developed seizures, manifesting as focal impaired awareness, and was treated with oxcarbazepine. She was developmentally and cognitively delayed, able to sit alone and walk with a walker, point and make some signs, but had no speech and could hold a pencil but not write. Asymmetric spastic quadriparesis (left more significant than right) with hypertonia and athetoid movements of the hands and fingers were noted on examination, as were a high palate, thin upper lip, and smooth philtrum. Her head circumference at 9 y was 51 cm (−0.73 SD), and she exhibited drooling and had feeding difficulties. Trio whole-exome sequencing (WES) revealed a de novo *ATP1A3* variant, c.2702G > T (p.Arg901Met), absent in both parents (Fig. 1 and *SI Appendix*, Fig. S1).

***Case B: Extensive bilateral PMG (c.2921+1G > A).*** Case B, a male child of nonconsanguineous parents from the Philippines, was born at 38-wk gestation. His head circumference at birth was 34 cm (−0.83 SD) and he developed seizures 12 h after delivery. Brain MRI at 6 wk revealed extensive bilateral PMG, and small, cyst-like areas were noted within the hippocampal heads and bodies. Video electroencephalograms (EEGs) confirmed a severe epileptic encephalopathy resistant to essentially all antiepileptic drugs. EEGs at 2 mo of age showed abundant electroclinical and electrographic seizures beginning predominantly from the right parasagittal region but also from the left and bilateral parasagittal regions. Visual and auditory evoked potential studies were normal at 4 and 5 mo of age, respectively. Evaluation at 14 mo revealed microcephaly, with a head circumference of 41.5cm (−4.63 SD), severe global developmental delay (never rolled over, sat up, or talked), intermittent nystagmus, significant axial and appendicular hypotonia, and hyporeflexia. Trio WES revealed a de novo *ATP1A3* variant, c.2921+1G > A, disrupting a conserved splice site, absent in both parents (Fig. 1*A* and *SI Appendix*, Fig. S1).

***Case C: Unilateral PMG (p.Leu924Pro).*** Case C, a male child of nonconsanguineous parents from Brazil, was born at 38-wk gestation by Cesarean section for fetal distress. He was hypotonic and noted to have a left clubfoot at birth and was admitted to neonatal intensive care when episodes of upward rolling of the eyes were noted on the first day of life. MRI revealed extensive cortical malformation of the right hemisphere with PMG comprising the frontal, parietal, and temporal right lobes and the insula, and a small focus of signal abnormality in the periventricular white matter, compatible with recent ischemic injury. EEG revealed the presence of electroclinical seizures and his neurological examination at the time disclosed episodic dystonic posturing of the upper left extremity alternating with excessive movements of closing his left hand with thumb adduction. He was discharged on phenobarbital and levetiracetam. Upon neurological examination at 8 mo of age, he had a head circumference of 42.5 cm (−1.75 SD), very poor eye contact, global hypotonia with present reflexes, absent head support, absence of rolling and of object gripping, and presence of babbling sounds. Trio WES revealed a de novo *ATP1A3* variant, c.2771T > C (p.Leu924Pro), absent in both parents (Fig. 1 and *SI Appendix*, Fig. S1).

***Case D: Extensive multifocal PMG (p.Gln851Arg).*** Case D, a male child of nonconsanguineous parents of European descent from the United States, was born at 41 wk by emergency Cesarean section; the pregnancy was complicated by fetal hydronephrosis. He developed electroclinical seizures and a neonatal encephalopathy requiring cooling and was discharged after 1 mo. MRI soon after birth showed multifocal PMG involving both cerebral hemispheres, right greater than left, with the right hemisphere smaller than the left (Fig. 1*A*). At 4 mo of age he was admitted for congenital hip dysplasia surgery and noted to have frequent breath-holding spells that worsened after the surgery. His varied seizure phenomenology included nystagmus, chin quivering, and hand shaking, which continue intermittently even through phenobarbital, levetiracetam, and oxcarbazepine combination therapy. At 15 and 30 mo of age, head circumference was 42.7 cm (−3.5 SD) and 44.2 cm (−3.3 SD), respectively. Physical examination at 18 mo demonstrated spastic hemiparesis involving primarily the left arm, but including the ipsilateral face and central hypotonia. Other symptoms included feeding difficulties and persistent constipation. WES revealed a de novo *ATP1A3* variant, c.2552A > G (p.Gln851Arg), absent in the mother (father was not available for testing).

**PMG-Associated *ATP1A3* Mutations Are Predicted to Disrupt Function.** *ATP1A3* encodes the P-type $Na^+$,$K^+$-ATPase α3-subunit (NM_152296), an integral membrane protein that relies on ATP hydrolysis to transport ions ($Na^+$ and $K^+$) via 10 membrane-inserted helices (tTM1 to TM10). This $Na^+$,$K^+$-ATPase is functionally supported by the β- and FXYD-subunits (7). *ATP1A3* has several conserved domains across α-isoform paralogs (α1 to α4) and orthologous genes (18), and is a highly constrained gene, with many fewer missense and LOF variants seen in the general population than predicted (gnomAD *z*-score of 6.33 and pLI score of 1.0, respectively). Taken together with *ATP1A3*'s known disease association with AHC, RDP, EIEE, and CAPOS (11), this suggests the identified variants in *ATP1A3* are likely disease-causing (*SI Appendix*, Table S1).

PMG-associated *ATP1A3* variants (p.Gln851Arg, p.Arg901-Met, p.Leu924Pro, and c.2921+1G > A), and an AHC variant with PMG (p.Leu888Pro) (17), occur at sites that are highly

GENETICS

conserved among the α-subunit paralogs (*ATP1A1* to *ATP1A4*) and invariant in other vertebrate *ATP1A3* orthologs (*SI Appendix*, Fig. S1*B*). In silico pathogenicity predictions for p.Gln851Arg, p.Arg901Met, p.Leu924Pro, and c.2921+1G > A suggest these variants are likely deleterious and disease-causing (*SI Appendix*, Table S1). Two amino acid substitutions reported here, Leu924-Pro and Gln851Arg, have been previously associated with EIEE and AHC without MCD (13, 19), further supporting the wide spectrum of *ATP1A3* phenotypes resulting from single amino acid variants (*SI Appendix*, Table S4). Leu924Pro pathogenicity has been demonstrated to affect ATPase trafficking to the plasma membrane, categorized functionally as LOF, leading to toxic effects in cells (13, 20). Together, the conservation of nucleotides, absence of variants in population databases, and previous LOF description of Leu924Pro (13, 20), suggest that these PMG *ATP1A3* alleles are likely pathogenic.

PMG-associated missense *ATP1A3* variants (p.Gln851Arg, p.Leu888Pro, p.Arg901Met, p.Leu924Pro) cluster within TM7 to TM8 segments (Fig. 1). The de novo *ATP1A3* variant in Case A, NM_152296.4:c.2702G > T, p.Arg901Met (R901M), affects an arginine in the extracellular loop connecting TM7 and TM8 (Fig. 1*C* and *SI Appendix*, Fig. S1*A*), in the same segment as a previously described variant (p.Leu888Pro) occurring in an AHC individual with PMG (17). Additionally, these PMG-associated amino acids, Arg901 and Leu888, are in close proximity to Glu899, Gln904, and Gln905, which interact with the Na,K-ATPase β-subunit (21), suggesting these variants may affect the critical α-β interaction necessary for membrane localization (Fig. 1*C*). Case C possesses a de novo *ATP1A3* variant, NM_152296.4:c.2771T > C, (p.Leu924Pro), altering an amino acid in the TM7 helix just upstream of the loop (Fig. 1*C*). Case D possesses a de novo *ATP1A3* variant, NM_152296.4:c.2552A > G, p.Gln851Arg, altering an amino acid in TM7 (Fig. 1*C*). The clustering of these missense variants between TM7 and TM8 suggests a disruption of specific protein–protein interactions; on the other hand, the de novo *ATP1A3* variant in Case B, NM_152296.4:c.2921+1G > A, abolishes the essential splice donor site of exon 21 (*SI Appendix*, Fig. S1), and similar *ATP1A3* splice site variants are known to cause AHC (22). Therefore, the PMG-associated variants found in Case B and Case C likely represent the most significant lost $Na^+$,$K^+$-ATPase functionality, with the most severe PMG patient phenotypes likely reflecting the most severe LOF effects (i.e., Case B, splice donor variant likely resulting in haploinsufficiency), compared to other less-severe *ATP1A3*-associated conditions. Importantly, the four de novo-affected individuals did not possess any alternative variants in known MCD genes or related MCD pathways.

***ATP1A3* mRNA Expression in the Human Fetal Neocortex.** To investigate the transcriptional trajectory of *ATP1A3* during human brain development underlying the prenatal phenotypes described in this study, we first contrasted the temporal expression patterns of *ATP1A1* to *-3* across brain regions (*ATP1A4* does not maintain any significant level of brain expression), mining bulk neocortical transcriptome data from the Allen Brain Atlas (23), ranging from 12 wk postconception (wpc) to adulthood (40-y-old) (Fig. 2*B*). We find that prenatal expression level of *ATP1A3* is higher than that of its paralogs (*ATP1A1* and *-2*), and *ATP1A3* persists postnatally (Fig. 2*B*). To gain further insights into the cell-biological mechanisms underlying the developmental cortical phenotypes described in this study, we characterized the patterns of *ATP1A3* expression in the midgestational fetal human neocortex (19 to 21 wpc). This developmental age offers a uniquely informative window into corticogenesis as many and diverse biological processes—including neurogenesis, neuronal migration and differentiation, and cortical folding—co-occur at this age. At this stage, early-born ENs have settled and started to differentiate within the innermost strata of the cortical plate (CP; prospective layers 6a-5), while later-born ENs progressively migrate past their predecessors to occupy the most superficial aspect of the CP (prospective layers 4-2) (24). A large fraction of upper-layer ENs are still being generated in the germinal zones, while others—en route to the CP—are withheld within the SP, a transient developmental layer crucial for corticogenesis, where ENs are primed by thalamic input and form transient synaptic connections with one another and with resident SP neurons (prospective layer 6b) (25).

To investigate *ATP1A3* expression in its tissue context, we performed RNA in situ hybridization (ISH) in coronal sections of fetal neocortex at 19 wpc from the perisylvian region, the area most commonly affected by PMG. *ATP1A3* mRNA was virtually undetectable in the germinal zones where dividing neural stem cells reside (ventricular and subventricular zone, VZ and SVZ), but abundant in postmitotic neuronal layers, with highest expression in the inner CP and SP (Fig. 2 *C* and *D*). Multiplexed fluorescent ISH analysis of *ATP1A3* with markers of two populations of cortical NPCs, radial glia, and intermediate progenitor cells, confirmed *ATP1A3* has low to zero expression in these dividing cells or their immediate progeny in either the VZ or the SVZ (Fig. 2*C*).

*ATP1A3*-associated diseases display a range of cerebellar deficits throughout childhood development (11, 26, 27). We therefore temporally profiled cerebellar *ATP1A3* expression from bulk RNA-seq data sampled from human embryonic week 12 to adult cerebellum (23). We show a differential enrichment of *ATP1A3* expression to the prenatal period, compared to *ATP1A1* and *ATP1A2*, yet *ATP1A3* also persists postnatally (Fig. 2*F*). To better understand *ATP1A3*'s developmental profile, we next performed ISH to evaluate *ATP1A3* expression in fetal cerebellum tissue (19 wpc), demonstrating an exclusive enrichment of *ATP1A3* within the Purkinje cell layer (Fig. 2*E*).

**Fetal Neocortex Single-Cell Analysis Demonstrates Robust *ATP1A3* Enrichment to Resident SP Neurons and Rostral Neocortical *ATP1A3* Enrichment.** Despite the high degree of compartmentalization of cell types into laminae, biological processes in the developmental neocortex are highly dynamic, and cellular compartments are heterogeneous in cell-type composition. scRNA-seq enables large-scale, simultaneous comparisons of gene expression across thousands of individual cells, thus bridging functional data from human genetics, immunohistochemistry, and cell-type–specific biology (28). Additionally, the limited spatial resolution of bulk RNA data from the Allen dataset does not allow cell-type identification within layers, which can result in miscategorized nonresident cells as they traverse layers (*SI Appendix*, Fig. S2*G*) (23). To this end, we performed Drop-seq on 125,942 individual cells from a 21-wpc human neococrtex (Fig. 3*A* and *SI Appendix*, Fig. S2*A*). Given the widespread pattern of PMG phenotypes from the perisylvian to frontal cortex localization described here, we sought to investigate *ATP1A3* expression across presumptive neocortical areal domains. To build our single-cell expression dataset, we collected cells from 11 adjacent sections spanning the dorsomedial and rostrocaudal axes of the neocortex, validating and refining the positional identity of these serial samples using the graded expression of cortical patterning genes as benchmarks (Fig. 3*A* and S2 *A–C*) (29). Using unsupervised statistical methods (*Materials and Methods*), cells were partitioned into four transcriptionally distinct clusters, which corresponded to the major neural cell classes in the midgestational neocortex: ENs, INs, NPCs, and glia (Fig. 3 *B* and *C* and *SI Appendix*, Fig. S2*D*). We excluded from this analysis all nonneural cell types as our scope of inquiry was specifically regarding *ATP1A3* dysfunction in neurons, and nonneural expression of *ATP1A3* is limited (Fig. 3*B* and *SI Appendix*, Fig. S2*D*). Within each of the main neuronal cell classes we could further resolve transcriptionally distinct cell subtypes and states, which we interpreted by the distinctive enrichment of marker genes in each group (*SI Appendix*, Fig. S2*D*). Among ENs, consistent with the

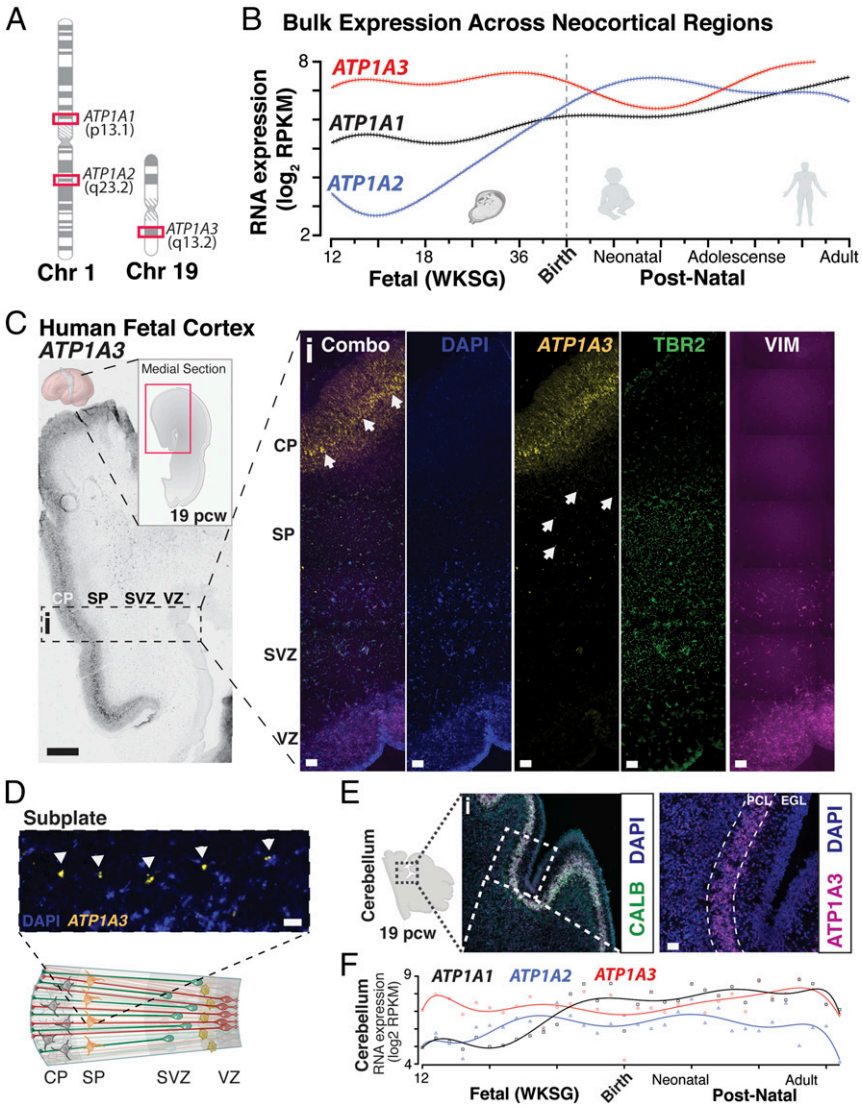


**Fig. 2.** *ATP1A3* is differentially enriched to the human fetal period across cortical layers. (*A*) Chromosome locations for CNS-enriched $Na^+,K^+$-ATPase α-isoforms, *ATP1A1* and *ATP1A2* (Chr1), and *ATP1A3* (Chr19). RPKM, reads per kilobase and million mapped reads. (*B*) RNA transcriptome analysis of bulk brain regions revealed *ATP1A3* transcripts are high during fetal gestation weeks (WKSG) and persist postnatally. CNS-expressed paralogous *ATP1A1* and *ATP1A2* paralogs show relative expression-pattern changes during development, while *ATP1A4* is not expressed significantly in the brain. (*C*, *Left*) *ATP1A3* mRNA chromogenic ISH performed on 19 wpc coronal brain sections demonstrate highest *ATP1A3* expression in the human CP and SP regions. (Scale bar, *Left*, 500 μm.) (*Right*) Corresponding fluorescence imaging of 19 wpc fetal brain with cell-type–specific markers for intermediate progenitors (TBR2) and neural progenitors (vimentin, VIM) demonstrates *ATP1A3* transcripts are not present within cells of the SVZ and VZ. Arrows indicate high expressing neurons in deep cortical layers and SP region. Scale bar, 50 μm. (*D*) Magnified image from *C* depicting high *ATP1A3*-expressing cells within the SP layer indicated with arrows. Scale bar, 50 μm. (*E*, *Left*) Schematic of developing sagittal fetal cerebellum tissue section at 19 wpc demonstrates enrichment of *ATP1A3* in Purkinje cell layer. (*i*) *ATP1A3* mRNA fluorescence in situ at 19 wpc demonstrates highest expression in the Purkinje cell layer, colocalizing with Purkinje cell marker calbindin (CALB1, green). (*ii*) Zoomed fluorescence image, including labeling of external granule layer. (Scale bar, *Left*, 50 μm.) DAPI stain for nuclei in blue. EGL, external granule layer; PCL, Purkinje cell layer. (*F*) Cerebellum RNA data revealed *ATP1A3* transcripts are high during fetal gestational weeks (WKSG) and persist postnatally. Raw transcriptome data for *B* and *F* from Allen Brain Atlas, presented as $log_2$ RPKM values and a polynomial fit to average across time points (23).

developmental landscape of midgestational corticogenesis described above, we could identify newborn and migratory upper-layer ENs at different stages of differentiation (clusters EN-0 to -3), and postmigratory deep-layer ENs expressing marker genes of maturing layer 6-5, including markers of resident SP neurons (EN-4) (Fig. 3*C*). Across fetal cortical regions, *ATP1A3* expression was observed in intermediate progenitor cell clusters, and more uniformly expressed in oligodendrocyte progenitor cells, INs, and ENs (Fig. 3*C* and *SI Appendix*, Fig. S2 *D* and *E*). Of these 18 cell types analyzed, the EN-4 cluster demonstrated the most significant *ATP1A3* enrichment and the focus for detailed analysis.

The EN-4 cluster was composed of cells sourcing from all cortical regions, and was marked by enriched expression of SP-specific genes (*CRYM* and *LPL*) (Fig. 3*C*), as well as by the expression of genes associated with neuronal maturation (e.g., axonal genes *NEFL*/*NEFM* and synaptic genes *SEMA3E*) (Fig. 3*H* and *SI Appendix*, Fig. S2*E*). This is consistent with the notion that the earliest-born neurons (a subset of which will persist in L6b in the adult cortex) settle and mature early in the developing SP (30). Within this cluster, *ATP1A3* appeared to be differentially expressed across the cortical region, with highest expression levels found in cells from frontal samples, intermediate levels in

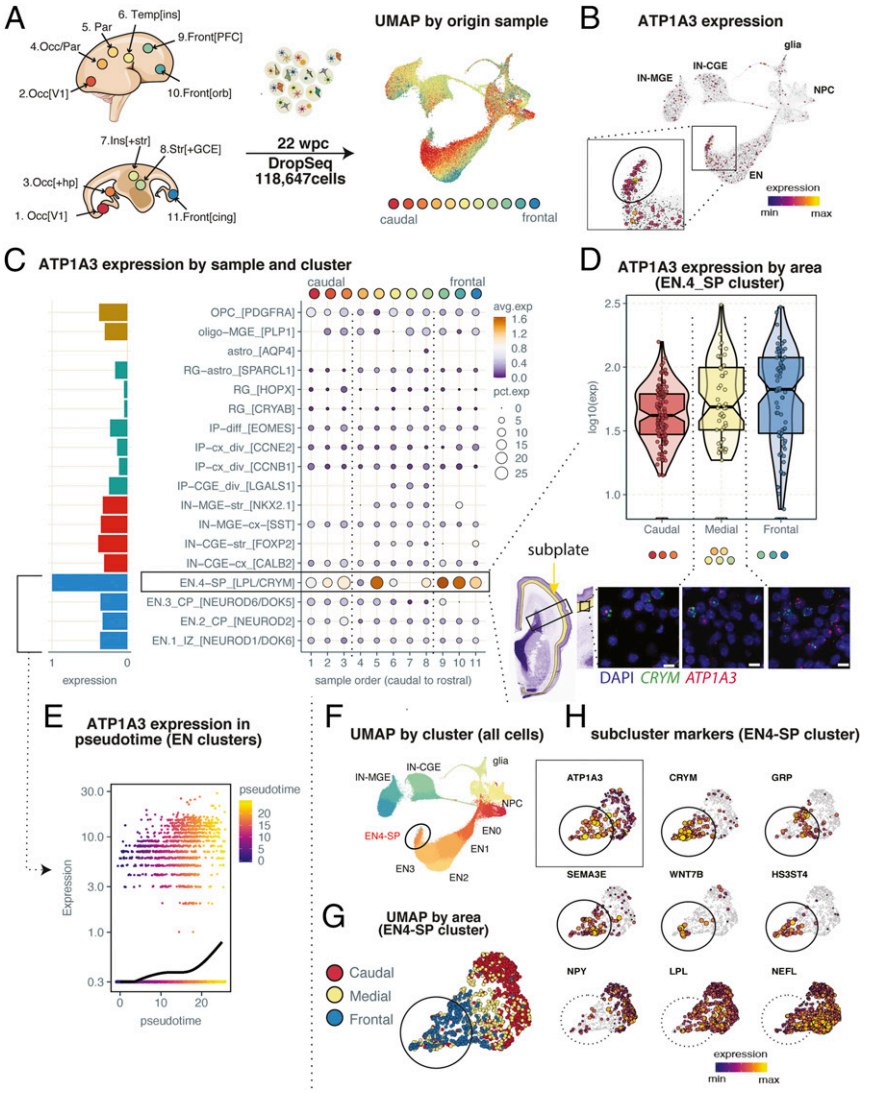


**Fig. 3.** Single-cell *ATP1A3* expression atlas in the developing human cerebral cortex. (*A*, *Left*) Schematic showing a 21-wpc forebrain and location of regions sampled (for anatomical detail, see *SI Appendix*, Fig. S2*A*). (*Upper*) Dorsolateral view; (*Lower*) sagittal view. (*Right*) Uniform Manifold Approximation and Projection (UMAP) of 125,943 single cells profiled by Drop-seq. Each dot represents a cell, color-coded by sample of origin. Key: blue-to-red: frontal-to-caudal. CGE, caudal ganglionic eminence; Hp, hippocampus; Ins, insula; MGE, medial ganglionic eminence; Occ, occipital; Orb, orbital; Par, parietal; PFC, prefrontal cortex; Str, striatum; Temp, temporal; V1, primary visual cortex. (*B*) UMAP plot of all profiled cells color-coded by level of *ATP1A3* expression. (*Inset*) UMAP region highlighting highest *ATP1A3* expression, which also maps onto ENs within the SP. (*C*, *Left*) Histogram showing relative expression of *ATP1A3* (*x* axis) across cell clusters (*y* axis). Notice enriched expression of *ATP1A3* in cluster EN.4-SP, containing SP EN neurons (see *H* and *SI Appendix*, Fig. S2*C* for SP markers enriched in this cluster). Mean *ATP1A3* expression was aggregated by cluster, then rescaled from 0 to 1. Cell clusters are color-coded by cell type (blue: EN; gold: glia; blue: IN; red: NPC). See *SI Appendix*, Fig. S2 *D* and *E* for cluster markers and assignments. (*Right*) Dot-plot showing *ATP1A3* expression across clusters split by areas of origin (*x* axis; sample 1–11, ordered from caudal to rostral). Color scale codes for mean expression by group; size of the dots codes for percentage of cells expressing *ATP1A3* in each group. (*D*, *Upper*) Violin-box plot showing differential expression of *ATP1A3* (*y* axis) in the EN-4–SP cluster across three main cortical partitions (*x* axis; caudal: samples 1 to 3, occipital cortex); medial: samples 4 to 8 (including parietal and temporal cortex, and subcortical structures); frontal: samples 9 to 11 (frontal cortex). Dots represent individual cells. Violins show probability density distributions; boxes show interquartile ranges; notches show confidence intervals around the median (horizontal lines). Outliers were trimmed. Mean expression of *ATP1A3* was aggregated by region, then $\log_{10}$-transformed. Notice the highest expression of *ATP1A3* in cells sampled from the frontal cortex, and lowest expression in cells sampled from caudal cortex. (*Lower*) Nissl-stained frontal coronal section of a 21-wpc forebrain highlighting anatomical position of SP. Source: Atlas of the Developing Human Brain, *BrainSpan* (www.brainspan.org) (64). *ATP1A3* mRNA ISH performed on 20-wpc coronal brain sections within the SP region to depict *ATP1A3* coexpression with EN.4_SP clade marker (*CRYM*). (Scale bar, 10 μm.) (*E*) *ATP1A3* expression across cells in the EN clusters (color-coded in blue in *C*, *Left*) ordered by pseudotime. Dots represent individual cells. *y* axis: log-transformed, scaled expression of *ATP1A3* by cell. *x* axis: pseudotime score (color-coded) for each cell, calculated using the Monocle3 algorithm. Trend-line shows the increase of *ATP1A3* expression as function of pseudotime, calculated by fitting a quasipoisson model to the data. (*F*) UMAP of all profiled cells color-coded by cluster (see *C*, *Left*). The EN-4–SP cluster is highlighted. (*G*) UMAP of cells in the EN-4–SP cluster (highlighted in *F*) color-coded by rostral, medial, and caudal anatomical partition of origin (see also *D*, *Upper*). Notice that cells segregate by origin. (*H*) Relative expression of areal marker genes in the EN-4–SP cluster (see *G*). Relative gene expression is coded by color and size. Notice that *ATP1A3* is enriched in cells expressing SP markers (*CRYM*, *WNT7B*, *HS3ST4*) and frontal cortex markers (*GRP*, *SEMA3E*), but not caudal cortex markers (NPY, LPL, NEFL).

cells from medial samples, and lowest levels in cells sampled from more caudal cortical regions (Fig. 3*C*). In agreement with this, expression of *ATP1A3* in the EN-4 cluster was found to be enriched in neurons coexpressing SP markers and frontal cortex markers, but much less so in neurons expressing caudal cortex markers (Fig. 3*D* and *SI Appendix*, Figs. S2 and S3).

Cortical development proceeds along a rostral-to-caudal maturation gradient, with asynchronous growth patterns accounting for the differential expansion of frontal and caudal cortical regions (31). This implies that, at any given time, neurons in frontal regions are on average more mature than their caudal counterparts. To investigate whether the observed *ATP1A3* enrichment in the EN-4 cluster might reflect a differential maturation state of EN neurons along the rostrocaudal axis, we performed pseudotime analysis of *ATP1A3* across all ENs (Fig. 3*E*). To do this, we used the Monocle3 algorithm, an established analytical tool allowing single-cell transcriptomes to be ordered and connected along a branched topology based on the differential expression of variable genes (32). By selecting an "origin" cell, this algorithm allows projection of a "pseudo-differentiation" trajectory onto the network topology (33). This analysis revealed a positive correlation between *ATP1A3* expression and EN differentiation, and may suggest that *ATP1A3* may be required during neuronal differentiation, as neurons transition to a mature state, most readily observed in resident SP neurons (Fig. 3*E*).

Finally, as the $Na^+$,$K^+$-ATPase is a heteromeric complex, we sought to identify potential isoform-specific and cell-type–specific vulnerabilities during corticogenesis; we compared the expression patterns of the *ATP1A1* to *-3* paralogs across cell clusters (*SI Appendix*, Fig. S3*A*). We found that expression of *ATP1A2* is restricted to NPCs (and specifically to radial glia), and is virtually undetectable in neurons, in an almost mutually exclusive pattern to *ATP1A3*. *ATP1A1* expression more closely mimicked *ATP1A3* expression, albeit its expression in NPCs was higher, and partially overlapped *ATP1A2* (*SI Appendix*, Fig. S3*A*). Accordingly, pairwise correlation analysis of the three isoforms across clusters revealed that expression of *ATP1A1* and *ATP1A3* correlates more strongly with the EN-4–SP cluster, while expression of *ATP1A1* and *ATP1A2* correlates more highly with NPC clusters (*SI Appendix*, Fig. S3 *B* and *C*). Across all cell-type clusters, pairwise correlation analysis indicated a positive correlation, though moderate, between *ATP1A1* and *ATP1A3*, but weak-to-no correlation between *ATP1A1* and *ATP1A2*, and between *ATP1A2* and *ATP1A3* (*SI Appendix*, Fig. S3 *B* and *C*). Interestingly, *ATP1A3* also seems to have an exclusive enrichment to interneurons, not shared by *ATP1A1*. Taking these data together, this analysis suggests that single-cell variable expression of $Na^+$,$K^+$-ATPase isoforms could underlie compensation or vulnerability mechanisms for disease haploinsufficiency or differential penetrance within specific cell populations. Finally, we analyzed a previously published smaller human fetal scRNA-seq data (34) (~4,300 cells), which lends support to our findings that *ATP1A3* is ubiquitously expressed across several cell types (*SI Appendix*, Fig. S9), with an EN enrichment.

***ATP1A3* Is Enriched in PV Interneurons and ENs in Infant Neocortex.** Given that *ATP1A3* expression persists in the postnatal neocortex (Fig. 2*B*), and that several known *ATP1A3* mutations show postnatal onset of symptoms, including epilepsy (11, 12), we profiled *ATP1A3* expression in the infant neocortex. Using Drop-seq, we profiled 51,878 nuclei from an ~8-mo-old human cortex, sampled from prefrontal, temporal, occipital, and parietal lobes (Fig. 4*A*). Unsupervised hierarchical clustering sorted nuclear transcriptomes into 3 major classes – ENs, INs, and glia – subdivided into 24 transcriptionally distinct cell classes (Fig. 4*A* and *SI Appendix*, Fig. S4). Within the EN clade, clusters stratified largely by layer and neuronal subtype, rather than cortical area, with several clusters enriched in gene markers of deep layers 5 and 6 (Fig. 4*B*; see *SI Appendix*, Fig. S4 for full clading). Within the IN clade, cells stratified by developmental origin (caudal or medial ganglionic eminence) and major "cardinal types," according to previous studies (35). In the infant neocortex, similar to the fetal neocortex, *ATP1A3* was enriched in neurons compared to glia, but unlike in the fetal dataset, *ATP1A3* was more highly expressed in INs than in ENs (Fig. 4*B* and *SI Appendix*, Fig. S5). Among neuronal clusters, and across cortical regions, *ATP1A3* expression was fairly variable, with the lowest expression in V1/occipital cortex cells, and wide range of expression levels within deep and upper layer EN clusters (Fig. 4*B*). However, no specific enrichment of *ATP1A3* expression was found in L6b ENs (i.e., the postnatal remnant of the fetal SP layer), suggesting that fetal enrichment of *ATP1A3* in the SP is developmentally transient, with maturation and migration of cells continuing to populate the upper layers. Of note, the lack of specific enrichment in postnatal SP may also reflect the fact that, unlike the fetal dataset, the postnatal dataset was built from nuclear RNA rather than whole-cell RNA, so that some transcripts may be underdetected.

Across IN clusters, expression of *ATP1A3* was highest in cells sampled from the frontal lobe (prefrontal BA10), and more strikingly so within $PV^+$ INs (Fig. 4*B* and *SI Appendix*, Fig. S4). This differential expression pattern raised the hypothesis that *ATP1A3* may be required dynamically across neuronal types, cell-biological processes, and across developmental ages. To gain insights into the nature of the cell-biological signature associated with *ATP1A3* expression, we compared the top 100 genes correlating with *ATP1A3* in EN and IN clusters. Interestingly, we found that 50 of 100 *ATP1A3*-correlating genes were shared across cell types, suggesting that *ATP1A3* partakes in similar transcriptional programs, and thus potentially similar function, in different neuronal types. In both ENs and INs, among the top genes correlating with *ATP1A3* was *FXDY6*, the FXYD-subunit of the ATPase complex (Fig. 4*D*). We did find, however, that the β-subunit *ATP1B1* (β1) correlated with *ATP1A3* only in ENs, and *ATP1B2* (β2) in INs, suggesting that, at least in part, *ATP1A3* may form cell-type–specific heteromeric ATPase complexes in different neuronal classes (Fig. 4*D* and S3 *A* and *B*). Gene ontology (GO) enrichment analysis of the top 100 genes most strongly correlated with *ATP1A3* in both ENs and INs revealed significant overrepresentation of gene products associated with TM ionic transport and the somatodendritic compartment, including dendrites and synapses (Fig. 4*D* and *SI Appendix*, Table S2). This is consistent with the established role of *ATP1A3* in synaptic transmission and membrane potential and suggests that *ATP1A3* may partake in a shared transcriptional network for which *ATP1A3* variants may perturb aspects of neuronal physiology central to many cell types at different stages of their maturation process.

Given the association of *ATP1A3* pathological variants with human disease phenotypes affecting higher-order cognitive functions with no clear counterpart in animal models, it was of interest to investigate the degree to which *ATP1A3* enrichment in INs may be conserved among humans, nonhuman primates, and rodents. We took advantage of a recently published scRNA-seq dataset profiling gene expression in homologous IN types in humans, nonhuman primates (macaques and marmosets), and mice (36). We found that relative *ATP1A3* expression levels across IN types, both in the neocortex and in the striatum, are largely conserved across species, with shared highest *ATP1A3* expression in the fast-spiking $PV^+$ INs (*SI Appendix*, Fig. S6). This suggests that the observed differential expression of *ATP1A3* across neuronal types is genetically encoded and evolutionarily conserved.

## Discussion

Mutations in *ATP1A3*, the gene encoding the Na,K-ATPase α3 catalytic subunit, have been associated with a wide spectrum of neurological diseases affecting childhood development, ranging in onset age from early infancy to late adolescence into adulthood.

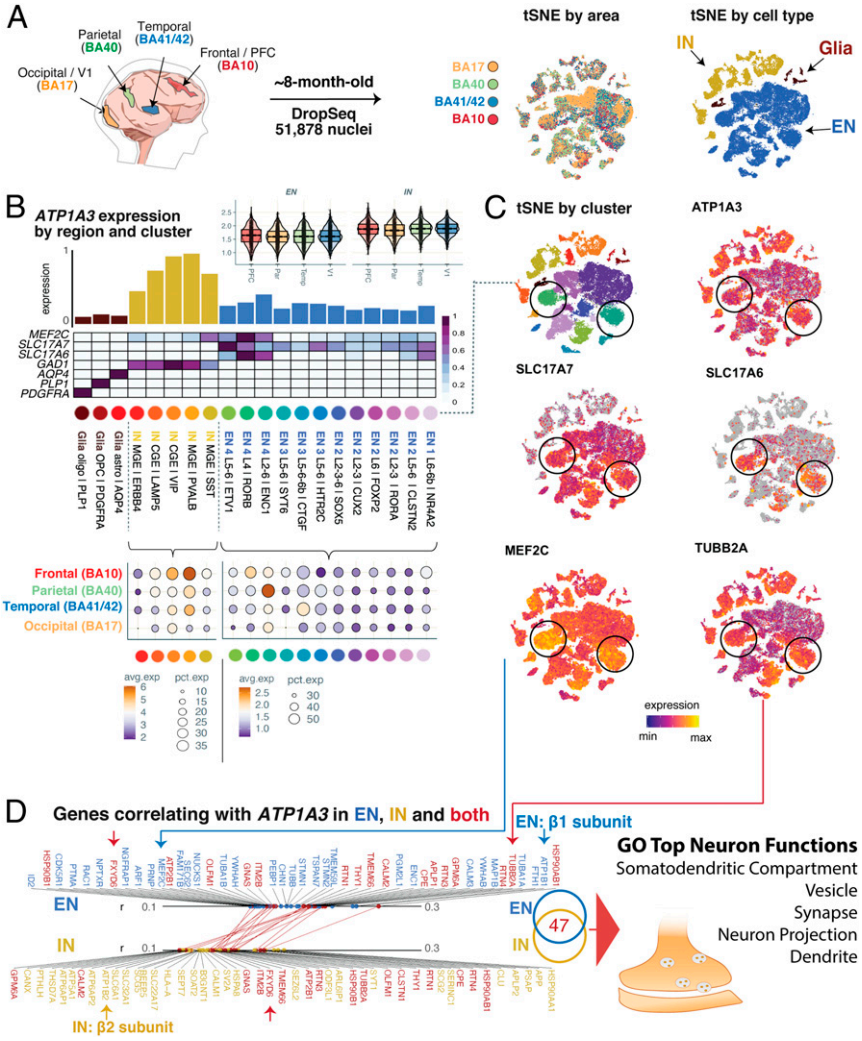


**Fig. 4.** Single-cell analysis of *ATP1A3* expression in the infant human neocortex. (*A*, *Left*) Schematic showing an 8-mo-old neocortex and location of regions sampled. BA: Brodmann area; PFC: prefrontal cortex; V1: primary visual cortex. (*Right*) t-distributed stochastic neighbor embedding (tSNE) of 51,878 single nuclei profiled by Drop-seq. Each dot represents a nucleus, color-coded by cluster (*Left*), cell type (*Center*), and origin sample (*Right*). See *C* for cluster and cell-class assignments. (*B*, *Left*) Dendrogram summarizing hierarchical clustering of data. Clusters are color-coded as in *A*, *Left*. See *SI Appendix*, Fig. S4 for cluster markers and assignments. (*Middle*) Bar graph showing relative expression of *ATP1A3* (*y* axis) across cell clusters (*x* axis). Mean expression was aggregated by cluster, then rescaled from 0 to 1 across all clusters. Data are color-coded by cell type (as in *A*, *Center*: blue, EN; gold, IN; brown, glia). (*Top Right*) Violin-box plot showing expression of *ATP1A3* (*y* axis) within EN and IN clusters across four main cortical partitions. *x* axis: caudal sample from occipital cortex (V1); medial samples from parietal (Par) and temporal (Temp) cortex; frontal samples from prefrontal cortex (PFC). Dots represent individual cells. Violins show probability density distributions; boxes show interquartile ranges; notches show confidence intervals around the median (horizontal lines). Outliers were trimmed. Mean expression of *ATP1A3* was aggregated by region, then $\log_{10}$-transformed. Notice the broad higher expression of *ATP1A3* in IN across *x* axis cortical regions, and lower expression in ENs. (*C*) tSNE plots showing specific enrichment of cortical marker genes including genes associated with early activity in the developing cortex (*MEFC2*, *SLC17A7*, and *SLC17A6*) (VGLU1 and VGLU2), and MCD-associated gene TUBB2A. (*D*) Venn diagram showing intersection between the top 100 genes correlating with *ATP1A3* in the EN cluster (blue) and IN cluster (gold); 47 of 100 genes are shared between the two groups. Top 50 genes correlating with *ATP1A3* in the EN and IN clusters are shown. Dots indicate Pearson's *R* for each gene in the EN cluster (*Upper*; blue) and IN cluster (*Lower*; gold). Genes found in both groups are indicated in red, and the respective correlation coefficients are connected by red lines. GO analysis for biological function of the 47 genes shared between EN and IN clusters indicates several components of the somatodendritic compartment, including synapses and dendrites (see *SI Appendix*, Tables S2 and S3 for entire GO table and *P* values).

Here, we describe *ATP1A3* pathogenic variants in individuals presenting with PMG, a severe prenatal malformation of the cerebral cortex characterized by abnormal gyrification and laminar organization. These findings extend the known phenotypic range of *ATP1A3*-related diseases and provide new insights into the molecular pathology of PMG and PMG-associated developmental channelopathies. Furthermore, by compiling a single-cell atlas of *ATP1A3* expression in the fetal and early postnatal neocortex, we revealed cell-type–specific *ATP1A3* expression in the fetal and infant human brain, establishing a spatiotemporal roadmap for future genotype–phenotype associations studies, and studies of *ATP1A3* function in the SP and cortical interneurons.

*ATP1A3*-associated conditions comprise a broad spectrum of overlapping phenotypes, including the blending of encephalopathies with more paroxysmal phenotypes, with a complex genotype–phenotype correlation. Further confounding genotype-to-phenotype studies, identical amino acid substitutions can impart variable presentations in humans (*SI Appendix*, Table S4); for example, Leu924Pro and Gln851Arg reported here have been previously associated with EIEE and AHC without MCDs (13, 19), but with postnatal microcephaly (Leu924Pro), suggesting pathogenic severity and susceptibility may differ between individuals. Differential penetrance between individuals may reflect α3 ATPase expression levels, competition between disease and

wild-type α3-subunits for utilization within Na,K-ATPases (13), and as described in this study, variable expression of α3 (and coexpression with other α- and β-subunits) within different cell populations (Fig. 4*D* and *SI Appendix*, Figs. S3 and S5). Individuals with heterozygous *ATP1A3* variants presented here with PMG also exhibited a range of phenotypic severity, from unilateral to extensive bilateral PMG, variable degrees of developmental delay, postnatal microcephaly, ataxia-like phenotypes, and EIEE. *ATP1A3*'s wide phenotypic spectrum is similar to known glutamate and sodium channel "developmental channelopathies," in which a subset of cases present with EIEE and developmental delay, both with and without MCDs and postnatal microcephaly (1). In a future opportunity to examine cortical tissue of PMG associated with *ATP1A3* variants, it would be useful to document cortical architecture, including whether gaps occur in the pia mater and glia limitans. This anatomical defect permits continuity between the molecular zones of adjacent microgyri for synaptic excitatory short-circuitry, leading to epilepsy, as with other genetic mutations in PMG (16).

Functional analysis of *ATP1A3* variants associated with postnatal diseases are largely described as LOF, including increased endoplasmic reticulum retention, reduced α3 expression, and disrupted cell morphology for L924P associated with EIEE (13, 20). Additional LOF mechanisms described associated *ATP1A3* disease-causing variants include changes in $Na^+$ affinity, impaired conformational changes, voltage-dependence shifts, and disruption of protein expression, among others (13, 37, 38). Since the Na,K-ATPase exports $Na^+$, and elevated $Na^+$ can be deleterious to cellular processes (39, 40) and is a known PMG-causing pathway (1, 4, 41), α3 variants that result in increased intracellular $Na^+$ concentration (e.g., a shift in $Na^+$ affinity or reduced ATPase in plasma membrane) could share this known PMG pathophysiology (1, 4, 41). This would suggest the toxicity resulting from inability to maintain sufficient levels of Na,K-ATPase, as observed with the deleterious splice variant likely causing haploinsufficiency (Case B), may also be correlated with patient phenotype severity (Individual B).

While some *ATP1A1* variants have been described to increase inward leak of $Na^+$ (42, 43), similar pathogenic gain-of-function effects have not been described in *ATP1A3*-related diseases. L924P may also activate a proapoptotic pathway (20), thus PMG pathophysiology could also reflect an accelerated activation of toxic downstream mechanisms that underlie postnatal *ATP1A3*-related disorders causing neurodegeneration or cell death, including postnatal microcephaly (44), regional neuronal loss (45), and cerebellar hypoplasia (26, 27). Moreover, two of the PMG-causing *ATP1A3* variants we describe are located in the α3 TM7/TM8 extracellular segment that interacts with the β-subunit (21) and Leu924Pro demonstrates β-subunit–associated LOF membrane localization properties (13, 20), suggesting the final formation of α-β complex could potentially underlie the observed pathophysiology. The β-subunit supports localization of the α-subunit to the plasma membrane and modulates affinity of $Na^+$ and $K^+$ for the ATPase (46), including a differential β1 vs. β2 effect on α-subunit ATPase pump activity (47). This suggests the observed cell-type–specific α-β combinations, including α3-β1 and α3-β2 enrichments in ENs and INs, respectively, could confer differential cell-type–specific pathology. Finally, α- and β-subunits can trigger intracellular signaling pathways associated with MCDs, including MAPK and AKT signaling via phosphoinositide 3-kinase (PI3K) and EGFR pathways, resulting in changes in cell polarity, growth, motility, and gene expression (48).

During embryonic brain development, bioelectric cellular properties are required for the propagation of key organizing signals, directly implicating ion channels and pumps in a variety of morphogenetic processes (15). For example, in mice and ferrets, experimental modulations in membrane potential and $Na^+$-dependent excitation have been linked to neuronal fate specification and directed migration (4–6, 49). Early electrical activity patterns in the SP accompany the dynamic formation of transient synaptic networks between resident SP neurons and migratory ENs and INs en route to the CP, ascending radial glia processes, and ingressing thalamic fibers (25). Thus, the SP acts to spatiotemporally integrate signals from many cellular sources. Our finding that 1) *ATP1A3*-expressing cells are located in the developing SP (ISH) (Fig. 3*D*), and 2) coexpress SP-specific marker genes (Drop-seq) (Fig. 4 and *SI Appendix*, Fig. S2) is therefore consistent with a role for *ATP1A3* in supporting electric activity within this compartment. This is also consistent with the notion that human SP neurons possess large $Na^+$ currents with prolonged depolarized states (50), and therefore require a stout mechanism to recover $Na^+$ and $K^+$ electrochemical gradients following excitation, a known function of the α3 ATPase in postnatal neurons (9, 10, 51). In addition, the finding that *ATP1A3*-expressing cells are also found in the inner aspect of the CP (ISH) (Fig. 2*C*), express L6-5 EN markers (Drop-seq) (Fig. 3*C*), together with the rostral-to-caudal gradient of *ATP1A3* expression and positive correlation with neuronal pseudoage (Monocle) (Fig. 3*F*), all are consistent with a role of *ATP1A3* in the maturation of early-born deep-layer ENs.

The observed differential prenatal expression of $Na^+$,$K^+$-ATPase isoforms (*ATP1A1* to *-3*) parallels the enrichment pattern reported for specific glutamate and sodium channel subtypes implicated in developmental channelopathies (1). These glutamate and sodium channel diseases result from mutations in developmental ion channel subtypes, specific channel subtypes that are utilized for developmental electrical functions (*SCN3A*, *GRIN2B*) (1), and contribute to neurotransmitters cellular responses (52), as opposed to others that support postnatal electrical functions (*SCN1A*, *GRIN2A*) (1). Similar to SCN3A and GRIN2B, the α3 isoform may have a similar specialized function in fetal brain neurons (compared to α1 isoforms), including interneurons. For example, $Na^+$ affinity is lower in α3 than α1 isoforms (39, 53), enabling α3-containing ATPase pumps to respond to larger $Na^+$ influxes. Lower $Na^+$ affinity provides a wider range to buffer aberrant $Na^+$ flux, therefore could provide an evolutionarily advantageous neuroprotective effect in cells during development. In addition to neurophysiological differences, known developmental channelopathy genes also maintain a robust cell type and subtype expression profiles as *ATP1A3*; for example, *SCN3A* and *GRIN2B* are enriched in ENs and some progenitor types (1, 4, 54), before transitioning to mostly *GRIN2A*-containing glutamate receptors and *SCN1A* in the postnatal cortex (1, 54). Moreover, the observed scRNA-seq *ATP1A2* enrichment in NPCs could offer a pathological basis for *ATP1A2* variants previously associated with fetal or early life demise, including microcephaly (55, 56).

In the postnatal cortex, the observed *ATP1A3* enrichment in interneurons likely supports physiological processes for maintaining inhibitory tone of cortical circuits (48), a proposed mechanism underling EIEE, or perhaps AHC. We were surprised to find that even after 90 million y of divergence, the human and rodent postnatal cortex possess similar single-cell distribution of *ATP1A3*, most notably in $PV^+$ INs, underscoring the utility of mice as a model for studying excitatory/inhibitory balance (57), especially in the context of PV IN loss relating to postnatal brain disorders (58). On the other hand, while *ATP1A3* IN expression appears to be conserved, species-specific differences in circuits and connectivity, and how interneurons shape gene expression differentially, could offer pathological differences between humans and mice, including early connections between SP and somatostatin/$PV^+$ cells (25, 30). For example, the observed PV IN enrichment of *ATP1A3* in the prefrontal cortex could contribute an early susceptibility for *ATP1A3* variant-associated childhood onset schizophrenia (12, 59). Intriguingly, the highest expressing *ATP1A3* cell types in the pre- and postnatal cortex (SP and $PV^+$ neurons), and Purkinje cells of the cerebellum, are all characterized by their robust firing properties (50, 60). Within these cell

types with more dynamic physiological needs, the low-affinity α3 would help maintain ionic gradients following excitation and suggests neurons with higher neurophysiological demands would be most susceptible to $Na^+$,$K^+$-ATPase dysfunction. In addition to differences between EN and IN $Na^+$,$K^+$-ATPase activity (61), differential $Na^+$,$K^+$-ATPase activity levels exists within mouse cortical pyramidal neurons in the postnatal brain (62). Taken together, the suspected LOF PMG-associated *ATP1A3* variants likely result in combined disruption of biosynthesis and pump dysfunction within vulnerable cell populations, with the most severe phenotype variants reflecting increased cytotoxicity capable of disrupting early neocortical developmental processes.

## Materials and Methods

**Human Subjects and Samples.** Individuals presented herein were identified and evaluated in a clinical setting, and biological samples collected after obtaining written informed clinical and research consent. Human subject research was conducted according to protocols approved by the institutional review boards of Boston Children's Hospital, Beth Israel Deaconess Medical Center, and the Mayo Clinic.

**Human Genetics Sequencing and Analysis.** For Cases A and B, WES and data processing were performed by the Genomics Platform at the Broad Institute of MIT and Harvard. Libraries from DNA samples (>250 ng of DNA, at >2 ng/μL) the Human Core Exome Kit from Twist Biosciences was used to capture target regions (~38-Mb target), and sequencing was performed on the Illumina NovaSEq. 6000 (150-bp paired reads) to cover >96% of targets at 20× and a mean target coverage of >100×. Sample identity quality-assurance checks were performed on each sample. See *SI Appendix* for additional information.

**Phenotypic Assessment.** All affected individuals and clinical data were examined by neurologists and geneticists and radiologists, and PMG was diagnosed using criteria described previously (1, 16). The *SI Appendix* summarizes their phenotypes and detailed clinical and radiographic evaluations.

**Human Brain Tissue Preparation and mRNA ISH.** Human brain tissue preparation and mRNA ISH were performed as previously described by Smith et al. (4). Briefly, following fixation (4% PFA) and cryoprotection (30% sucrose), brains were frozen using isopentane on dry ice. Samples were sectioned at 20- to 30-μm thickness (Leica Cryostat), mounted immediately onto warm charged SuperFrost Plus slides (Fisher), and stored at –80 °C. We followed the manufacturer's standard protocol for multiplex fluorescent ISH (Multiplex v2 kit, Advanced Cell Diagnostics). See *SI Appendix, Supplemental Materials and Methods* for more details.

**Bulk Human Cortex Gene-Expression Analysis.** The Allen Human Brain Atlas (ABA) publishes a rich dataset of cortical genetic expression across cortical brain regions, from age 8 wpc to adult ages (23). BrainSpan data analysis of *ATP1A1* (chr1:116,915,289–116,952,883, GRCh37/hg19), *ATP1A2* (chr1:160,085,548–160,113,381, GRCh37/hg19), and *ATP1A3* (chr19:42,470,733–42,498,384, GRCh37/hg19) was performed. *ATP1A4* is not expressed in the CNS and was not included as the read counts were near zero. See *SI Appendix, Supplemental Materials and Methods* for more details.

**Drop-Seq Isolation and Sequencing.** Single-nucleus and single-cell suspensions were processed for Drop-seq as described in detail (5, 6), with modifications detailed by Krienen et al. (36) (see *SI Appendix* for additional details). Single-cell cDNA libraries were processed and sequenced using Illumina short-read sequencing on a Nova-seq platform at the Broad Institute. Libraries were sequenced at an average depth of >8 reads per unique molecular identifier (UMI). Sequencing reads were aligned to the hg19 human reference genome. For the fetal dataset, only reads mapping to exons were used; for the postnatal dataset, reads mapping to both exons and introns were used. Software and core computational analysis for alignment and downstream processing of Drop-seq sequencing reads are freely available at https://github.com/broadinstitute/Drop-seq. Cell selection was performed as described previously (63). See *SI Appendix, Supplemental Materials and Methods* for independent component analysis, clustering, and statistical analysis details.

**Graphics.** Graphics were prepared in Adobe Illustrator and using BioRender software.

**Data Availability.** Sequencing data have been deposited in dbGap, https://www.ncbi.nlm.nih.gov/gap/ (accession no. phs001272.v1.p1) (65). Supplemental data tables are available at https://figshare.com/s/64b648891e4817efb123. All other data are included in the main text and *SI Appendix*.

**ACKNOWLEDGMENTS.** We thank the participant families presented here and members of the C.A.W. laboratory for helpful discussions; Johnathan Hecht for assistance with human tissue; and Kathleen Sweadner for productive discussion. Human tissue was obtained from the NIH NeuroBioBank at the University of Maryland. This research was supported by NIH F32NS100033801 and K99NS112604 (to R.S.S.), NIH T32GM007753 (to S.K.A.), NIH R01NS032457 and R01NS035129 (to C.A.W.); Boston Children's Hospital Intellectual and Developmental Disabilities Research Center U54 HD090255; and by the Allen Discovery Center program, a Paul G. Allen Frontiers Group-advised program of the Paul G. Allen Family Foundation. Sequencing and analysis were provided by the Broad Institute of MIT and Harvard Center for Mendelian Genomics and was funded by the National Human Genome Research Institute, the National Eye Institute, and the National Heart, Lung, and Blood Institute Grant UM1 HG008900 to Daniel MacArthur and Heidi Rehm. Additional support was provided from the Tommy Fuss Foundation (R.S.S and J.G.-H.). C.A.W. is an Investigator of the HHMI.

1. R. S. Smith, C. A. Walsh, Ion channel functions in early brain development. *Trends Neurosci.* **43**, 103–114 (2020).
2. K. Platzer *et al.*, *GRIN2B* encephalopathy: Novel findings on phenotype, variant clustering, functional consequences and treatment aspects. *J. Med. Genet.* **54**, 460–470 (2017).
3. A. E. Fry *et al.*, De novo mutations in GRIN1 cause extensive bilateral polymicrogyria. *Brain* **141**, 698–712 (2018).
4. R. S. Smith *et al.*, Sodium channel SCN3A ($Na_V1.3$) regulation of human cerebral cortical folding and oral motor development. *Neuron* **99**, 905–913.e7 (2018).
5. I. Vitali *et al.*, Progenitor hyperpolarization regulates the sequential generation of neuronal subtypes in the developing neocortex. *Cell* **174**, 1264–1276.e15 (2018).
6. N. Hurni *et al.*, Transient cell-intrinsic activity regulates the migration and laminar positioning of cortical projection neurons. *Cereb. Cortex* **27**, 3052–3063 (2017).
7. R. Holm *et al.*, Neurological disease mutations of α3 $Na^+$,$K^+$-ATPase: Structural and functional perspectives and rescue of compromised function. *Biochim. Biophys. Acta* **1857**, 1807–1828 (2016).
8. K. M. McGrail, J. M. Phillips, K. J. Sweadner, Immunofluorescent localization of three Na,K-ATPase isozymes in the rat central nervous system: Both neurons and glia can express more than one Na,K-ATPase. *J. Neurosci.* **11**, 381–391 (1991).
9. J. Kim *et al.*, Calmodulin mediates Ca2+ sensitivity of sodium channels. *J. Biol. Chem.* **279**, 45004–45012 (2004).
10. L. D. Picton, F. Nascimento, M. J. Broadhead, K. T. Sillar, G. B. Miles, Sodium pumps mediate activity-dependent changes in mammalian motor networks. *J. Neurosci.* **37**, 906–921 (2017).
11. A. Brashear, K. J. Sweadner, J. F. Cook, K. J. Swoboda, L. Ozelius, ATP1A3-related neurologic disorders. GeneReviews Internet (1993). https://www.ncbi.nlm.nih.gov/books/NBK1115/. Accessed 24 July 2020.
12. N. Smedemark-Margulies *et al.*, A novel de novo mutation in ATP1A3 and childhood-onset schizophrenia. *Cold Spring Harb. Mol. Case Stud.* **2**, a001008–a001013 (2016).
13. E. Arystarkhova *et al.*, Factors in the disease severity of ATP1A3 mutations: Impairment, misfolding, and allele competition. *Neurobiol. Dis.* **132**, 104577 (2019).
14. C. Q. Simmons *et al.*, Direct evidence of impaired neuronal Na/K-ATPase pump function in alternating hemiplegia of childhood. *Neurobiol. Dis.* **115**, 29–38 (2018).
15. M. Levin, G. Pezzulo, J. M. Finkelstein, Endogenous bioelectric signaling networks: Exploiting voltage gradients for control of growth and form. *Annu. Rev. Biomed. Eng.* **19**, 353–387 (2017).
16. A. C. Jansen *et al.*, The histopathology of polymicrogyria: A series of 71 brain autopsy studies. *Dev. Med. Child Neurol.* **58**, 39–48 (2016).
17. F. Gurrieri, F. D. Tiziano, G. Zampino, G. Neri, Recognizable facial features in patients with alternating hemiplegia of childhood. *Am. J. Med. Genet. A.* **170**, 2698–2705 (2016).
18. M. V. Clausen, F. Hilbers, H. Poulsen, The structure and function of the Na,K-ATPase isoforms in health and disease. *Front. Physiol.* **8**, 371 (2017).
19. M. Masoud *et al.*, Motor function domains in alternating hemiplegia of childhood. *Dev. Med. Child Neurol.* **59**, 822–828 (2017).
20. E. Arystarkhova, L. J. Ozelius, A. Brashear, K. J. Sweadner, Misfolding, altered membrane distributions, and the unfolded protein response contribute to pathogenicity differences in Na,K-ATPase *ATP1A3* mutations. *J. Biol. Chem.* **296**, 100019 (2020).
21. T. Shinoda, H. Ogawa, F. Cornelius, C. Toyoshima, Crystal structure of the sodium-potassium pump at 2.4 A resolution. *Nature* **459**, 446–450 (2009).
22. L. Viollet *et al.*, Alternating hemiplegia of childhood: Retrospective genetic study and genotype-phenotype correlations in 187 subjects from the US AHCF registry. *PLoS One* **10**, e0127045 (2015).
23. A. R. Jones, C. C. Overly, S. M. Sunkin, The Allen Brain Atlas: 5 years and beyond. *Nat. Rev. Neurosci.* **10**, 821–828 (2009).
24. J. A. Miller *et al.*, Transcriptional landscape of the prenatal human brain. *Nature* **508**, 199–206 (2014).

25. H. J. Luhmann, S. Kirischuk, W. Kilb, The superior function of the subplate in early neocortical development. *Front. Neuroanat.* **12**, 97 (2018).
26. K. J. Sweadner *et al*., ATP1A3 mutation in adult rapid-onset ataxia. *PLoS One* **11**, e0151429 (2016).
27. J. Uchitel *et al*., The epileptology of alternating hemiplegia of childhood. *Neurology* **93**, e1248–e1259 (2019).
28. E. Z. Macosko *et al*., Highly parallel genome-wide expression profiling of individual cells using nanoliter droplets. *Cell* **161**, 1202–1214 (2015).
29. T. Sun *et al*., Early asymmetry of gene transcription in embryonic human left and right cerebral cortex. *Science* **308**, 1794–1798 (2005).
30. A. Hoerder-Suabedissen, Z. Molnár, Molecular diversity of early-born subplate neurons. *Cereb. Cortex* **23**, 1473–1483 (2013).
31. P. Rakic, Neurons in rhesus monkey visual cortex: Systematic relation between time of origin and eventual disposition. *Science* **183**, 425–427 (1974).
32. J. Cao *et al*., The single-cell transcriptional landscape of mammalian organogenesis. *Nature* **566**, 496–502 (2019).
33. J. G. Camp *et al*., Human cerebral organoids recapitulate gene expression programs of fetal neocortex development. *Proc. Natl. Acad. Sci. U.S.A.* **112**, 15672–15677 (2015).
34. T. J. Nowakowski *et al*., Spatiotemporal gene expression trajectories reveal developmental hierarchies of the human cortex. *Science* **358**, 1318–1323 (2017).
35. C. Mayer *et al*., Developmental diversification of cortical inhibitory interneurons. *Nature* **555**, 457–462 (2018).
36. F. M. Krienen *et al*., Innovations in primate interneuron repertoire. *bioRxiv* [Preprint] (2019). https://www.biorxiv.org/content/10.1101/709501v1 (Accessed 24 July 2020).
37. E. L. Heinzen *et al*.; ATP1A3 Working Group, Distinct neurological disorders with ATP1A3 mutations. *Lancet Neurol.* **13**, 503–514 (2014).
38. M. Li *et al*., A functional correlate of severity in alternating hemiplegia of childhood. *Neurobiol. Dis.* **77**, 88–93 (2015).
39. G. Azarias *et al*., A specific and essential role for Na,K-ATPase $\alpha 3$ in neurons co-expressing $\alpha 1$ and $\alpha 3$. *J. Biol. Chem.* **288**, 2734–2743 (2013).
40. M. S. Toustrup-Jensen *et al*., Relationship between intracellular Na+ concentration and reduced Na+ affinity in Na+,K+-ATPase mutants causing neurological disease. *J. Biol. Chem.* **289**, 3186–3197 (2014).
41. T. Zaman *et al*., SCN3A-Related neurodevelopmental disorder: A spectrum of epilepsy and brain malformation. *Ann. Neurol.* **88**, 348–362 (2020).
42. E. A. B. Azizan *et al*., Somatic mutations in ATP1A1 and CACNA1D underlie a common subtype of adrenal hypertension. *Nat. Genet.* **45**, 1055–1060 (2013).
43. M. Kaneko, B. S. Desai, B. Cook, Ionic leakage underlies a gain-of-function effect of dominant disease mutations affecting diverse P-type ATPases. *Nat. Genet.* **46**, 144–151 (2014).
44. A. R. Paciorkowski *et al*., Novel mutations in ATP1A3 associated with catastrophic early life epilepsy, episodic prolonged apnea, and postnatal microcephaly. *Epilepsia* **56**, 422–430 (2015).
45. A. L. Oblak *et al*., Rapid-onset dystonia-parkinsonism associated with the I758S mutation of the ATP1A3 gene: A neuropathologic and neuroanatomical study of four siblings. *Acta Neuropathol.* **128**, 81–98 (2014).
46. G. Blanco, G. Sánchez, R. W. Mercer, Differential regulation of Na,K-ATPase isozymes by protein kinases and arachidonic acid. *Arch. Biochem. Biophys.* **359**, 139–150 (1998).
47. F. Hilbers *et al*., Tuning of the Na,K-ATPase by the beta subunit. *Sci. Rep.* **6**, 20442 (2016).
48. Z. Li, S. A. Langhans, Transcriptional regulators of Na,K-ATPase subunits. *Front. Cell Dev. Biol.* **3**, 66 (2015).
49. J. J. LoTurco, D. F. Owens, M. J. Heath, M. B. Davis, A. R. Kriegstein, GABA and glutamate depolarize cortical progenitor cells and inhibit DNA synthesis. *Neuron* **15**, 1287–1298 (1995).
50. A. R. Moore *et al*., Electrical excitability of early neurons in the human cerebral cortex during the second trimester of gestation. *Cereb. Cortex* **19**, 1795–1805 (2009).
51. C. Vaillend, S. E. Mason, M. F. Cuttle, B. E. Alger, Mechanisms of neuronal hyperexcitability caused by partial inhibition of Na+-K+-ATPases in the rat CA1 hippocampal region. *J. Neurophysiol.* **88**, 2963–2978 (2002).
52. S. Mayer *et al*., Multimodal single-cell analysis reveals physiological maturation in the developing human neocortex. *Neuron* **102**, 143–158.e7 (2019).
53. M. Dobretsov, J. R. Stimers, Neuronal function and alpha3 isoform of the Na/K-ATPase. *Front. Biosci.* **10**, 2373–2396 (2005).
54. I. Bagasrawala, F. Memi, N. V Radonjic, N. Zecevic, N-methyl d-aspartate receptor expression patterns in the human fetal cerebral cortex. *Cereb. Cortex* **27**, 5041–5053 (2017).
55. N. Chatron *et al*., A novel lethal recognizable polymicrogyric syndrome caused by ATP1A2 homozygous truncating variants. *Brain* **142**, 3367–3374 (2019).
56. F. P. Monteiro *et al*., Biallelic loss of function variants in ATP1A2 cause hydrops fetalis, microcephaly, arthrogryposis and extensive cortical malformations. *Eur. J. Med. Genet.* **63**, 103624 (2020).
57. P. Bøttger *et al*., Distribution of Na/K-ATPase alpha 3 isoform, a sodium-potassium P-type pump associated with rapid-onset of dystonia parkinsonism (RDP) in the adult mouse brain. *J. Comp. Neurol.* **519**, 376–404 (2011).
58. A. S. Hunanyan *et al*., Mechanisms of increased hippocampal excitability in the Mashl$^{+/-}$ mouse model of $Na^+$ /$K^+$ -ATPase dysfunction. *Epilepsia* **59**, 1455–1468 (2018).
59. B. Chaumette *et al*., Missense variants in ATP1A3 and FXYD gene family are associated with childhood-onset schizophrenia. *Mol. Psychiatry* **22**, 539 (2018).
60. R. Tremblay, S. Lee, B. Rudy, GABAergic interneurons in the neocortex: From cellular properties to circuits. *Neuron* **91**, 260–292 (2016).
61. K. S. Richards, K. Bommert, G. Szabo, R. Miles, Differential expression of Na+/K+-ATPase alpha-subunits in mouse hippocampal interneurones and pyramidal cells. *J. Physiol.* **585**, 491–505 (2007).
62. T. R. Anderson, J. R. Huguenard, D. A. Prince, Differential effects of Na+-K+ ATPase blockade on cortical layer V neurons. *J. Physiol.* **588**, 4401–4414 (2010).
63. A. Saunders *et al*., Molecular diversity and specializations among the cells of the adult mouse 703 brain. *Cell* **174**, 1015–1030.e16 (2018).
64. Alan Institute for Brain Science, BrainSpan, Atlas of the Developing Human Brain, http://www.brainspan.org/. Accessed 24 July 2020.
65. R. Smith, C. Walsh, Human genetics sequencing data. National Center for Biotechnology Information (NCBI) dbGap. https://www.ncbi.nlm.nih.gov/gap/?term=phs001272.v1.p1. Deposited 1 May 2021.